

Dynamic Force Microscopy in Fluid

M. Lantz,¹ Y. Z. Liu,² X. D. Cui,² H. Tokumoto¹ and S. M. Lindsay^{2,*}

¹ Joint Research Center for Atom Technology, c/o National Institute for Advanced Interdisciplinary Research, 1-1-4 Higashi, Tsukuba, Ibaraki 305-0046, Japan

² Department of Physics and Astronomy, Arizona State University, Tempe, AZ 85287-1504, USA

Low-amplitude dynamic force microscopy can operate in a non-contact mode, sensing changes in liquid properties near a surface. Operation of the microscope in water at the higher amplitudes often required for stable imaging has been investigated. When driven by direct application of a force to the tip, the microscope is stable over a wide range of operating frequencies. At low frequency, the interfacial stiffness extracted from approach curves is found to be of the order of 1 N m^{-1} on first contact, which is indicative of imaging via a compressed liquid layer. Measurements of the spectral response of the cantilever and numerical simulations confirm this and show that viscous damping at the surface also plays a role. Copyright © 1999 John Wiley & Sons, Ltd.

KEYWORDS: liquid–solid interface; atomic force microscopy; dynamic force microscopy

INTRODUCTION

Dynamic force microscopy (DFM) has become the method of choice for imaging soft materials in liquid, arguably one of the most important applications of atomic force microscopy. The mechanism of DFM in air has received considerable attention,^{1–3} as has the operation of DFM on clean surfaces in a vacuum.⁴ The interaction between an oscillating cantilever and a solid surface in fluid has been studied with the cantilever driven solely by thermal fluctuations⁵ or at a very low amplitude of oscillation.^{6–8} Recently, O'Shea *et al.* demonstrated that low-amplitude DFM senses changes in the elastic and viscous properties of the surface at nanometer distances, and can therefore be operated in a non-contact mode. The purpose of this paper is to discuss operation of DFM at the larger amplitudes typical of many imaging applications.^{10,11}

Both operation of the microscope and investigation of its imaging mechanism are complicated by the heavy viscous damping and mass loading of the cantilever. Butt first showed that the resonant frequency of a cantilever in water is reduced by about a factor of three compared to that in air as a consequence of its increased effective mass due to the need to move fluid with the cantilever.¹² The mechanical Q factor is also reduced by many orders of magnitude by viscous damping.¹² These first studies utilized the thermal fluctuations of a cantilever far from the surface. As the cantilever is brought towards a surface, the effective viscosity of the fluid increases rapidly owing to the need for fluid to be squeezed out of the gap between cantile-

ver and surface.^{5,13} However, the effect does not contribute to image contrast because it is approximately constant once the cantilever is close enough for the tip to be nearly in contact with the surface.⁷ Our concern here is with the changes that occur at nanometer distances from the surface.

This paper is organized as follows: the criteria for choosing operating amplitude are presented and a procedure for amplitude calibration is outlined; the mechanical difference between acoustic excitation of the cantilever and direct drive by magnetic deflection is demonstrated with approach curves; a formula for interpreting low-frequency, high-amplitude approach curves is derived and applied to surfaces under water; and measurements of the cantilever response as a function of frequency and distance from a mica surface are presented and interpreted with the aid of numerical simulations. These confirm the interpretation of the low-frequency approach curves, which indicate that on initial 'contact' the tip is sensing the surface via compression of an interfacial fluid layer. Thus, it appears to be possible to operate DFM in non-contact mode in fluid even at high amplitude.

EXPERIMENTAL

Measurements were made with two systems. One was a Seiko (Tokyo) atomic force microscope with a home-made liquid cell equipped with a ferrite-cored solenoid beneath the sample. Rectangular silicon cantilevers (Olympus, Tokyo) with nominal spring constant (k), of 2 and 20 N m^{-1} were modified by the addition of a small magnetic particle as described elsewhere.⁹ The other was a MAC Mode Pico scanning probe microscope

* Correspondence to: S. M. Lindsay, Department of Physics and Astronomy, Arizona State University, Tempe, AZ 85287-1504, USA.

that utilized silicon nitride cantilevers (nominal stiffness 0.6 N m^{-1}) coated with a magnetic film (MAC Levers), both from Molecular Imaging (Phoenix, AZ). The instrument was equipped with a piezo-electric drive to permit switching between magnetic and acoustic excitation of the cantilever. We used flame-annealed gold (111) films and clean water¹⁴ or freshly-cleaved mica in water from a Millipore system.

OPERATING AMPLITUDE FOR DFM IN LIQUID

It is desirable to operate DFM at as small an amplitude and with as small a setpoint change as possible, in order to minimize disturbance of the sample. This may be seen by considering the energy dissipated in the sample on each cycle in the low-frequency limit:

$$\Delta E(z) = \frac{1}{2}k\{A_0^2 - [A_0 - A(z)]^2\} \quad (1)$$

where k is the cantilever spring constant, A_0 is the amplitude immediately prior to approach to the surface and $A(z)$ is the amplitude at some distance z from a nominal surface plane (see below). In contrast to DFM in a vacuum or air, resonance effects are small, so the microscopy is largely sensitive to changes in amplitude. Its sensitivity is thus limited by thermal fluctuations and is not significantly enhanced by operating at resonance. However, stable operation requires an amplitude sufficient to pull the tip out of attractive interactions (such as adhesion). In addition to the usual requirement that $(\partial F_{ts}/\partial z)^{\text{max}} < k$, we need

$$kA_- + F_M + F_{ts}^{\text{max}} < 0 \quad (2)$$

where A_- is the amplitude on the down swing (Fig. 1), F_M is the maximum magnetic force (for the case of magnetic drive) and F_{ts}^{max} is the tip-sample maximal interaction force. In non-contact operation tip-sample adhesion can be avoided, but in normal imaging conditions on rough surfaces a safe value of A_0 is $\sim 2\text{--}5 \text{ nm}$ with $k \sim 1 \text{ N m}^{-1}$.

It is common practice to calibrate the oscillation amplitude by pushing the cantilever far into the surface and assuming that, in hard contact, the amplitude falls one nanometer for every nanometer the tip advances (i.e. $dA/dz = 1$; see Fig. 1 for definition of quantities). This procedure assumes that the bending profiles in oscillation and contact are the same. Although this is not true in general,¹⁵ we found that for the cantilevers used in this work the decay of the oscillation amplitude followed the deflection trace in contact (for low driving frequencies). This is illustrated in Fig. 2(a), which shows that the bending signal with the tip is driven at 1 kHz, which is well below the resonant frequency of 14.8 kHz. The lower part of the swing lies on the line drawn through the contact part of the signal for which $dA/dz = 1$. (Note that we have arbitrarily set the position of the onset of amplitude decay to be zero.) This is not the case at higher frequencies. The ratio dA/dz for the same cantilever, driven at resonance is 1.64 [Fig. 2(b)]. Here, we have used the data from Fig. 2(a) to calibrate the amplitude signal from which this gradient is derived. The increased gradient comes about from the dissipation of stored energy, as is clear from the decay of

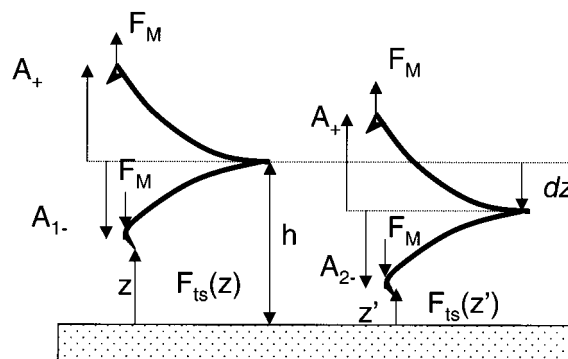


Figure 1. Showing an oscillating cantilever a distance h above a surface (left) and a distance $h - dz$ (right) above a surface. The extent of the swing is A_+ in the upward direction and A_{1-} (left) or A_{2-} (right) in the downward direction. The tip-surface force is F_{ts} and the maximum force exerted by the applied magnetic field is F_m .

both the top and bottom portions of the swing. The Q for this cantilever ($k = 2 \text{ N m}^{-1}$) was ~ 3 . When a higher Q cantilever ($Q = 12$, $k = 20 \text{ N m}^{-1}$) is driven at resonance, the gradient approaches 2, which is the limit appropriate for symmetrical decay of the amplitude [Fig. 2(c)]. Thus an initial calibration at low frequency

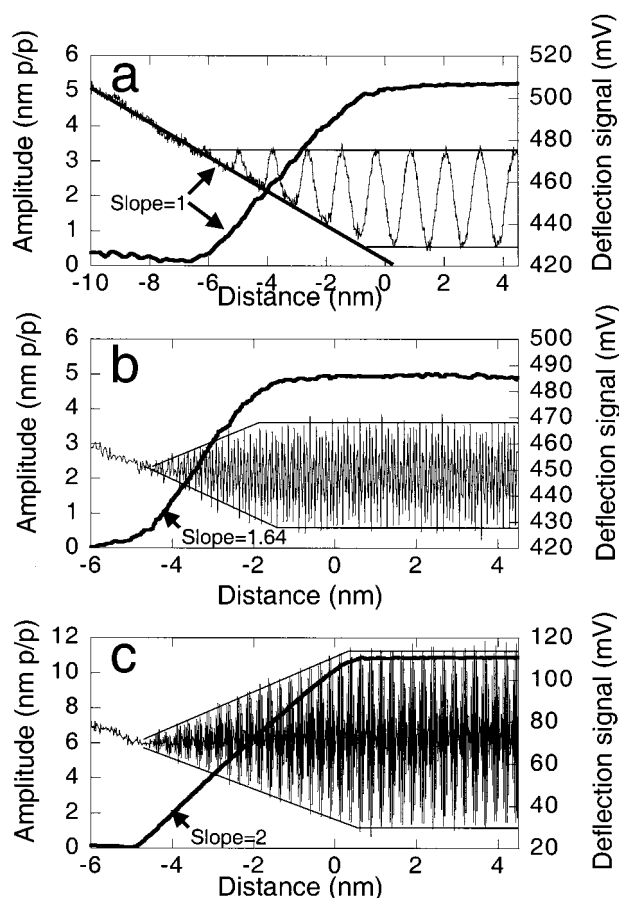


Figure 2. Plots of bending signal (measured as a signal in mV) as the cantilever was advanced towards a mica surface in water. Data for the oscillation amplitude were acquired simultaneously. (a) An Si tip with $k = 2 \text{ N m}^{-1}$ and a resonant frequency of 14.8 kHz driven at 1 kHz. (b) The same tip as (a) at resonance. (c) A 20 N m^{-1} cantilever driven at resonance. The envelope of the oscillation has been outlined in order to emphasize the asymmetry in curves (a) and (b).

is required because the gradient near resonance is not known *a priori*.

ACOUSTIC VERSUS MAGNETIC DRIVE

It is well known that acoustic drive in liquid is restricted to frequencies at which the cantilever holder resonates, resulting in many sharp response peaks despite the dampened response of the cantilever.^{16,17} These spurious responses can be eliminated with magnetic drive.¹² However, magnetic drive appears to offer advantages that go beyond an increased range of operating frequency. It is claimed that the technique gives a better signal-to-noise ratio and images with higher resolution.^{10,11,18} This may be related to the different process by which the cantilever is bent in the two cases. In magnetic excitation, the cantilever and sample remain fixed, the cantilever being bent directly by application of a magnetic force or magnetostriction [see inset, Fig. 3(a)]. In acoustic excitation, the long-wavelength sound waves cause displacement of the cantilever holder [inset, Fig. 3(b)] so that the net bending signal is the difference between displacement of the tip and displacement of the holder. Writing the complex amplitude in this way and solving for the real part of the signal yields the following result

$$A(\omega) = A_0 \sqrt{\frac{\omega^4 + (\omega\omega_0/Q)^2}{(\omega^2 - \omega_0^2)^2 + (\omega\omega_0/Q)^2}} \quad (3)$$

Here A_0 is the amplitude of the drive applied to the holder, ω_0 is the resonant frequency of the cantilever and Q is the quality factor of the cantilever. Note that the response, $A(\omega)$, drops to zero at zero frequency, in contrast to magnetic drive where the response is F_M/k .¹¹

Figure 3(a) shows amplitude curves for approach and retraction for magnetic drive together with simultaneously acquired average displacement curves (calibrated in nN). Note that on initial approach (1) dA/dz was less than unity but approached it closer in (2). The signal eventually fell to zero within the noise level (3) as the displacement signal rose (4), indicating

hard contact. In this case the tip was then pushed far ($\sim 1 \mu\text{m}$) into the surface, resulting in adhesion on retraction (5). The oscillation amplitude remained at zero until the tip jumped out of contact (6). On further retraction, the deflection signal remained at zero but the amplitude continued to grow, suggesting that in region 2 the tip is 'out of contact' with the surface.

Figure 3(b) shows approach curves for acoustic drive near resonance (25 kHz) and well below it (5 kHz). In this case, bending is induced by displacement of the cantilever holder. At resonance ($Q = 3$) the holder must be displaced 0.3 nm for every nanometer of tip motion. Thus, even in hard contact, a residual signal is generated as the moving cantilever holder bends the cantilever (indicated by the double arrow below the approach curve). Far from resonance, more complex behavior is observed. For very low frequencies, the bending signal goes to zero (which is what prevents precise amplitude calibration in this case). However, residual bending driven by motion of the cantilever holder yields a signal in contact, so the sense of the servo signal is reversed [Fig. 3(b)]. One cause of the reported differences in image quality may be the difficulty of amplitude control with acoustic drive.

HARMONIC AND ANHARMONIC ANALYSIS OF LOW-FREQUENCY DATA

O'Shea *et al.*^{7,9} have analyzed data for low-amplitude operation using a damped harmonic oscillator model of the cantilever motion in which the displacement amplitude $A(z, \omega)$ is given by

$$A(z, \omega) = \frac{F_M}{\sqrt{[k + \bar{S}(z) - \bar{m}^*(z)\omega^2]^2 + \frac{[k + \bar{S}(z)]\bar{m}^*(z)\omega^2}{Q(z)^2}}} \quad (4)$$

where F_M is the magnitude of the applied magnetic force, k is the cantilever spring constant, $\bar{S}(z)$ is an effective interface stiffness, $\bar{m}^*(z)$ is an effective cantilever mass and $Q(z)$ is the mechanical Q factor. The bars over

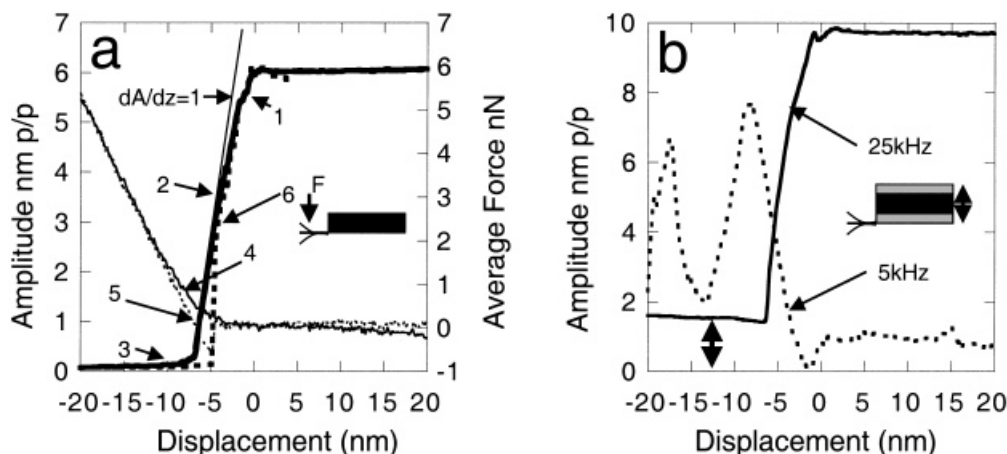


Figure 3. Approach curves for a silicon nitride tip and an Au(111) surface in water. (a) Magnetic excitation at 5 kHz (resonance = 35 kHz) with the amplitude calibrated as described in the text. The heavy line shows the approach signal and the heavy dotted line shows the retraction signal. The thin solid line shows the approach force, averaged over the tip motion, and the thin dashed line shows the same quantity in retraction. (b) Acoustic drive for a drive peak (25 kHz) near resonance (heavy solid line) and well below (5 kHz, dashed line) resonance. The double arrow below the 25 kHz trace shows the residual signal. Amplitude calibration was assumed to be the same as in (a) but this could not be checked. Note that the signal sense is reversed at low frequency. Insets illustrate the displacements in the two cases.

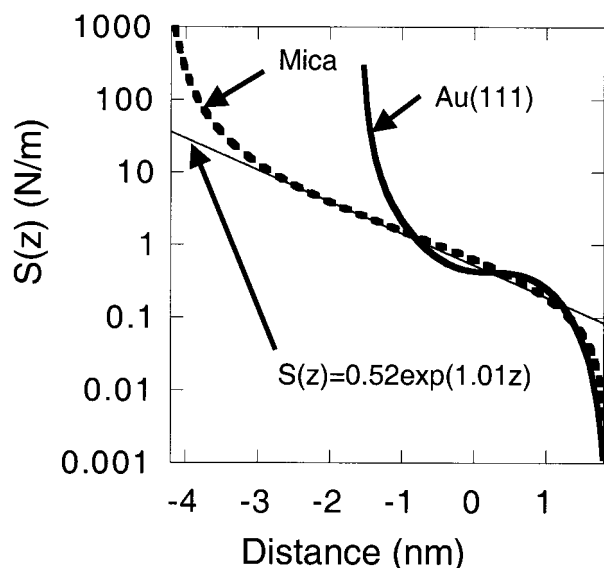


Figure 4. Interfacial stiffness $S(z)$ for mica and a silicon tip (dashed line) and Au(111) and a silicon nitride tip (heavy line) in water. Results were calculated from low-frequency approach curves using Eqn. (7). The thin line indicates a region of exponential decay.

S , m^* and Q indicate that they are averaged over the motion of the cantilever, which is accurate for small amplitudes. This approximation breaks down at high amplitude. For example, the low-frequency limit of (4) yields the well-known result $A_0/A(z) = [S(z) + k]/k$,¹⁹

implying that the *fractional* change in amplitude is constant at a given z . This is obviously not true at high amplitude, where all of the motion that lies beyond the range of surface forces is unaffected by the approach.

It is relatively straightforward to generalize the result of Pethica and Oliver¹⁹ to the high-amplitude regime. Consider a cantilever initially at a height h above a surface (Fig. 1) with a maximum upward swing $A_{1+} = F_M/k$ and a maximum downward swing A_{1-} . Moved a distance dz towards the surface (Fig. 1), the new downward swing is A_{2-} . With $dA = A_{1-} - A_{2-}$ and $z' = z - (dz - dA)$ the force equilibration on the downward stroke is given by

$$F_M = kA_{1-} + F_{ts}(z) = kA_{2-} + F_{ts}[z - (dz - dA)] \quad (5)$$

where we have assumed a symmetric magnetic drive so that the magnitude of the magnetic force on the downward swing is equal to that on the upward swing. If we define a differential force 'constant' $S(z)$ by

$$S(z) = \frac{F_{ts}[z - (dz - dA)] - F_{ts}[z]}{(dA - dz)}, \quad (dA - dz) \rightarrow 0 \quad (6)$$

then Eqn. (5) yields

$$S(z) = \frac{k}{\left[\frac{dz}{dA}(z) - 1 \right]} \quad (7)$$

with repulsive forces defined as negative. Thus, the inverse of the derivative of the approach curve taken at

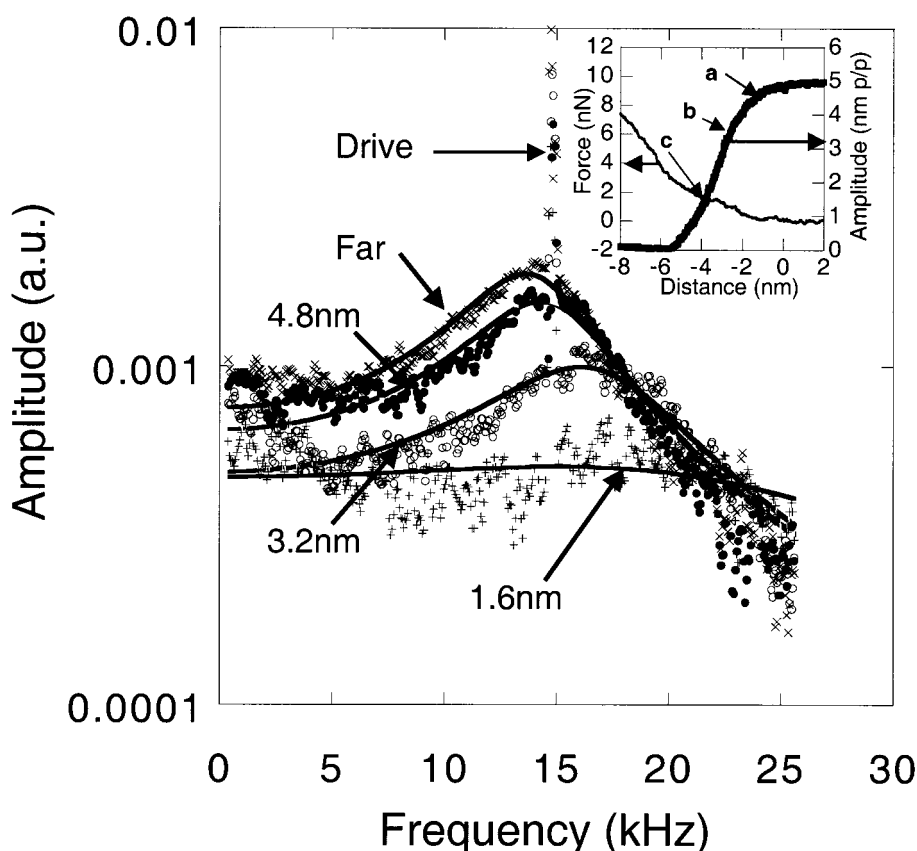


Figure 5. Amplitude vs. frequency for various nominal distances from the surface (as indicated) for a 5 nm peak-to-peak drive for a silicon tip approaching mica in water. Note the logarithmic scale. The drive signal (just above resonance) is off-scale, and the data are obtained with a small amount of white noise added to the drive so that the 'small signal' analysis is conducted as an average over large amplitudes. The solid lines are fits to Eqn. (4). Inset shows the approach and average force curves, indicating the set points used to obtain the spectral data ($a = 4.8$ nm, $b = 3.2$ nm, $c = 1.6$ nm).

low frequency may be used to estimate $S(z)$. The approach curves of Figs 2(a) and 3(a) were used to generate the values for $S(z)$ displayed in Fig. 4. Curves were fitted to a ninth-order polynomial that was then differentiated explicitly and the results used in Eqn. 7. The procedure becomes unreliable as dA/dz approaches unity, but both systems show that, at the extreme low point of the swing, S is initially of the order of 1 N m^{-1} for distances of the order of nanometer. This is characteristic of compression of a fluid layer.^{7,8,20} Closer to the surface $S(z)$ rises rapidly to values of the order of 100 N m^{-1} , which is characteristic of indentation of a solid surface by a tip.^{19,21} The data for mica exhibit an extended region of single exponential behavior, indicated by the line of Fig. 4.

AMPLITUDE DECAY OVER A WIDE FREQUENCY RANGE

The measurements of O'Shea *et al.*⁹ were extended into the high-amplitude regime by driving a silicon cantilever just above its resonant frequency (14.8 kHz) with sinusoidal excitation that produced a 5 nm peak-to-peak deflection when the cantilever was far from the surface. A small amount of white noise was added to the drive signal and the deflection signal was fed into a spectrum analyzer. Far from the surface ($\sim 500 \text{ nm}$) this yields a response that fits the damped harmonic oscillator model (Eqn. 4) with $k = 2.5 \text{ N m}^{-1}$, $\bar{m}^*(z) = 3.1 \times 10^{-10} \text{ kg}$ and $\bar{Q}(z) = 2.4$, although there is some discrepancy at low frequencies (Fig. 5). This is to be expected because these measurements are averages over large-amplitude motion. Surprisingly, Eqn. (4) fits the data to about the same extent even as the surface is approached. The distance was controlled using amplitude damping at the drive frequency (inset, Fig. 5). We arbitrarily took 5 nm from the initial onset of decay to be the surface location so that at *a* (inset, Fig. 5) the tip was 4.8 nm, at *b* it was 3.2 nm and at *c* it was 1.6 nm from it. The fits were made with $\bar{m}^*(z)$ approximately constant, with $\bar{Q}(z)$ remaining ~ 2 (falling to 0.9 for the 1.6 nm curve). Values of $\bar{S}(z)$ were 0.4 N m^{-1} (4.8 nm), 1.4 N m^{-1} (3.2 nm) and 1.5 N m^{-1} (1.6 nm). The numbers are of no significance beyond their role in parameterizing the response curves; the surprising result is that Eqn (4) fits to any degree.

A NUMERICAL MODEL

A large-amplitude model must be solved in order to interpret the data of Fig. 5 and a simple model is shown schematically in Fig. 6. The mass m (representing the cantilever) is shown displaced from its equilibrium position at $Z = 0$ to hit the mass M (representing the interface), depressing it by an amount δ from its equilibrium position. At the low point of the swing, $\delta = A_+ - A_-$ (see Fig. 1). The equilibrium height of the tip above the surface is h' (see Fig. 6), related to the h of Fig. 1 by some unknown constant displacement. We model the interfacial stiffness with a single exponential for simplicity, $S(\delta) = S_0 \exp(\delta/\lambda)$, as an approximation

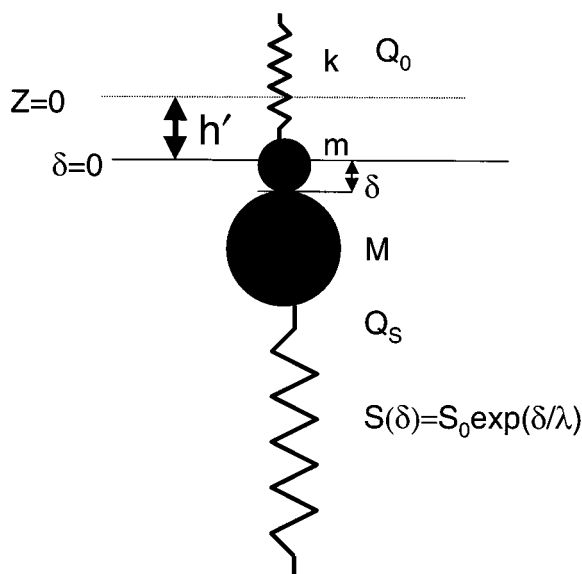


Figure 6. Model of the tip-surface interaction. The equilibrium height of the tip above the 'surface' is h' . The tip (mass m) is shown displacing the 'surface' (mass M) by an amount δ .

to the results of the low-frequency analysis (Fig. 4) and consistent with other observations on liquid-solid interfaces.⁸ Approach curves in organic solvents have shown that interfacial viscosity plays a dominant role.⁹ In water, however, the relatively small changes in the shape (i.e. Q) of the response curves on approach, combined with the role of interfacial stiffness in the low-frequency data (Fig. 4), suggest that interfacial stiffness is important. Thus we treat Q_0 and Q_s as constants, recognizing that $Q_s < 1$ indicates increased viscous damping at the surface. We explored the effects of varying the surface mass M but obtained good fits with a constant value. Non-zero mass is required in order to produce the abrupt change in tip motion at the surface [see Figs 2(a) and 8] but it must be small enough to give a resonant frequency for the model surface ($\sqrt{S_0/M}$) that is well above the resonant frequency of the cantilever. This was achieved with $M = 6 \times 10^{-12} \text{ kg}$. This parameter may be of less importance in a two-exponential model, which would give a more accurate representation of the measured interfacial stiffness (Fig. 4), but the present approach minimizes the number of model parameters.

The equation of motion of the system is

$$m^* \ddot{Z} + \gamma^* \dot{Z} + k^* Z = F_0 \exp i\omega t \quad (8)$$

where Z is measured from the equilibrium position of the tip and, for Z_+ and

$$\begin{aligned} |Z_-| < h': m^* &= m, \quad k^* = k, \quad \gamma^* = \gamma_c \\ |Z_-| \geq h': m^* &= M, \quad k^* = k + S_0 \exp(\delta/\lambda), \\ &\gamma^* = \gamma_c + \gamma_s \end{aligned}$$

where Z_- is the displacement on the downward stroke and Z_+ is the displacement on the upward stroke. The damping parameters are given by $\gamma_c = m\omega_0/Q_0$ and $\gamma_s = M\omega_s/Q_s$. Equation (8) was integrated numerically to obtain $Z(t)$, starting from $Z(0) = 0$, $\dot{Z}(0) = 0$ and $\ddot{Z}(0) = 0$; F_0 was chosen to be 1.25 nN with $k = 2.5$

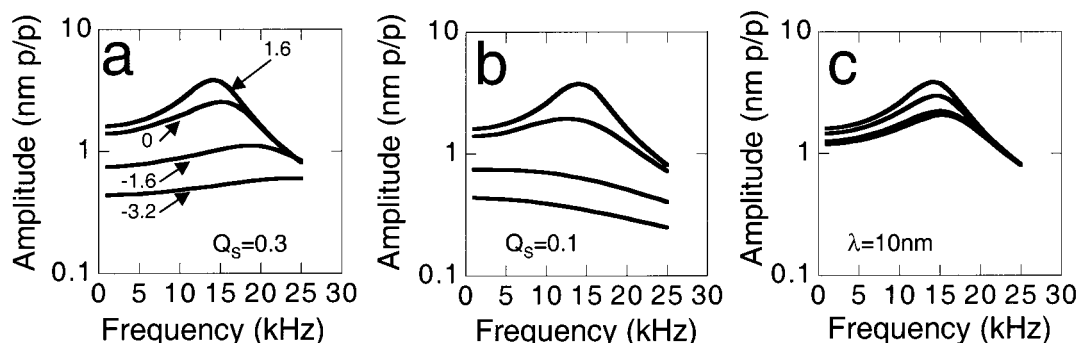


Figure 7. Some simulations of the spectral response for a peak-to-peak amplitude of 2 nm at low frequency and the parameters described in the text. The amplitude scale is logarithmic. At $h' = 1.6$ nm (top curves) the tip barely touches the 'surface'. Lower curves are calculated for steps of 1.6 nm towards the 'surface'.

N/m^{-1} to give a low-frequency half-amplitude of 2 nm; and m was calculated from the free resonant frequency to be 3.1×10^{10} Kg. Each cycle of oscillation was divided into 60 000 time increments and the equations were integrated over 40 complete cycles. A comparison of the results after 20 and 40 cycles showed that a steady state was reached at 20 cycles, so subsequent calculation was stopped at this time. Calculations were carried out for $h' = 1.6, 0, -1.6$ and -3.2 nm. The first value barely touches the surface ($A^+ - h' = 0.4$ nm), whereas the last value corresponds to an equilibrium position well into the region of increased stiffness.

Some results are displayed in Fig. 7. The best agreement [Fig. 7(a)] was obtained with the experimentally determined form $S(z) = 0.52 \exp(1.01\delta)$ and with $Q_s = 0.3$. Results are quite sensitive to Q_s , as illustrated in Fig. 7(b). A small decrease (to 0.1) results in an apparent decrease of peak frequency with penetration because of the frequency dependence of the damping. Further reduction results in a very 'non-harmonic' response, the top of the peak near resonance being cut off as the tip loses energy to the surface. A higher Q_s value results in too sharp a peak at the greatest penetration depth.

The simulation are also quite sensitive to the form of the surface stiffness. This can be demonstrated by changing either S_0 or λ , and we show plots for $\lambda = 10$ nm in Fig. 7(c). These show that the amplitude damping

and frequency shift are too small in this case. The opposite results are obtained with an increase in S_0 or a decrease in λ .

The shape of the tip trajectory calculated with these parameters is in reasonable agreement with measurements, as shown in Fig. 8 (data and calculations are for 5 kHz drive). The cut-off appearance of the bottom requires both some surface mass and a surface stiffness that increases strongly with distance.

DISCUSSION AND CONCLUSIONS

Both the simple analysis of low-frequency approach curves and numerical modeling of the spectral response show that, at the lowest point of its swing, the tip senses an initial interfacial stiffness of the order of 1 N m^{-1} even at the nanometer amplitudes used for DFM imaging. This value is characteristic of fluid compression.^{7,8,20} Thus, operated at small changes in amplitude, DFM in fluid is non-contact, confirming and extending the low-amplitude results of O'Shea *et al.*⁹ This conclusion is in accord with experience in operating the microscope. A small setpoint amplitude reduction does not, in general, give the best resolution. Resolution increases as the amplitude reduction is increased, until the interaction becomes so strong, that the underlying sample is disturbed. This suggests that the best operating conditions for the microscope are obtained with the smallest free amplitude (A_0) that yields stable operation together with the largest amplitude reduction that does not disturb the sample. Softer cantilevers would help this process, but we have found that the background signal owing to cantilever motion in contact becomes significant when the stiffness falls below 0.1 n m^{-1} .

Our results, and those of O'Shea *et al.*,⁹ suggest an interfacial stiffness for water that is much greater than that implied by a recent simulation²² that yielded piconewton changes over subnanometer distances. We cannot exclude the possibility that contamination plays some role²³ because of the non-UHV environment. None the less, our measurements were carried out in relatively cleaner conditions than those used for imaging biological molecules, for example.

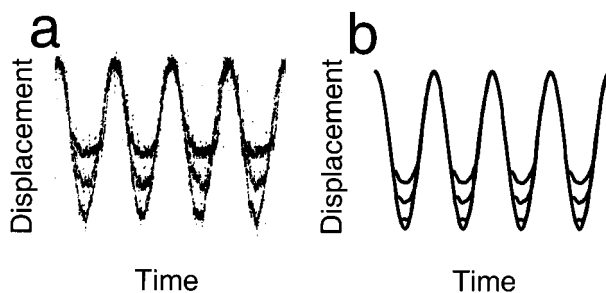


Figure 8. (a) The experimentally measured tip bending signals at 5 kHz as the setpoint is increased stepwise (data overlaid). (b) Calculated displacement with the parameters used for calculation of the data in Fig. 7(a).

The simulations suggest that, at least for the initial approach, the dominant contribution arises from stiffening of the water at the interface, in contrast to the dominant role of viscosity in other cases⁹ (though the viscous contribution clearly increases at short distances). Thus DFM images in water, particularly at low frequency, may be interpreted as a map of contours of constant stiffness. The value of the setpoint stiffness may be evaluated from the approach curve using Eqn. (7). The remarkably 'harmonic' appearance of the high-amplitude spectral response is accidental. We would not

expect it at a more dissipative interface. Measurements like these on more complex surfaces, such as tethered polymers,⁵ might be expected to yield information on both elastic and viscoelastic properties of the interface.

Acknowledgements

We have received support from the Japanese New Energy and Technology Development Organization (NEDO), the NSF (BIR 9513233) and the Molecular Imaging Corporation (TCL-157C).

REFERENCES

1. J. Tamayo and R. Garcia, *Langmuir* **12**, 4430 (1996).
2. J. Tamayo and R. Garcia, *App. Phys. Lett.* **71**, 2394 (1997).
3. B. Anczykowski, D. Kruger, K. L. Babcock and H. Fuchs, *Ultramicroscopy* **66**, 251 (1996).
4. F. J. Giessibl, *Phys. Rev. B* **56**, 16010 (1997).
5. A. Roters, M. Gelbert, M. Schimmel, J. Ruhe and D. Johannsmann, *Phys. Rev. E* **56**, 3256 (1997).
6. S. J. O'Shea, R. M. Atta and M. E. Welland, *Rev. Sci. Instrum.* **66**, 2508 (1995).
7. S. J. O'Shea and M. E. Welland, *Langmuir* **14**, 4186 (1998).
8. W. Han and S. M. Lindsay, *Appl. Phys. Lett.* **72**, 1656 (1998).
9. S. J. O'Shea, M. A. Lantz, and H. Tokomoto, *Langmuir* in press (1998).
10. M. A. Lantz, S. J. O'Shea and M. E. Welland, *Appl. Phys. Lett.* **65**, 409 (1994).
11. W. Han, S. M. Lindsay and T. Jing, *Appl. Phys. Lett.* **69**, 4111 (1996).
12. H. J. Butt, P. Siedle, K. Seifert, K. Fendler, T. Seeger, E. Bamberg, A. L. Weisenhorn, K. Goldie and A. Engel, *J. Microsc.* **169**, 75 (1993).
13. J. A. Williams, *Engineering Tribology*. Oxford University Press, New York (1994).
14. T. Wandlowski, D. Lampner and S. M. Lindsay, *J. Electroanal. Chem.* **404**, 215 (1996).
15. J. E. Sader, I. Larson, P. Mulvaney and L. White, *Rev. Sci. Instrum.* **66**, 3789 (1995).
16. C. A. J. Putman, K. O. V. d. Werf, B. G. deGroot, N. F. V. Hulst and J. Greve, *Appl. Phys. Lett.* **64**, 2454 (1994).
17. T. E. Schaffer, J. P. Cleveland, F. Ohnesorge, D. A. Walters and P. K. Hansma, *J. Appl. Phys.* **80**, 3622 (1996).
18. W. Han, S. M. Lindsay, M. Dlakic and R. E. Harrington, *Nature (London)* **386**, 563 (1997).
19. J. B. Pethica and W. C. Oliver, *Phys. Scr.* **T19**, 61 (1987).
20. A. Dhinojwala and S. Granick, *J. Chem. Soc. Faraday Trans.* **92**, 619 (1996).
21. D. Sarid, *Atomic Force Microscopy* (Oxford University Press, New York (1992)).
22. K. Koga and X. C. Zeng, *Phys. Rev. Lett.* **79**, 853 (1997).
23. T. Smith, *J. Colloid Interface Sci.* **75**, 51 (1980).